


## Article

# Design of Semiconductor Contact Grating Terahertz Source with Enhanced Diffraction Efficiency

Zoltán Tibai <sup>1</sup>, Nelson M. Mbithi <sup>1,2</sup>, Gábor Almási <sup>1,2</sup>, József A. Fülöp <sup>3</sup> and János Hebling <sup>1,2,4,\*</sup> <sup>1</sup> Institute of Physics, University of Pécs, Ifjúság ú. 6, 7624 Pécs, Hungary<sup>2</sup> Szentágotthai Research Centre, University of Pécs, Ifjúság ú. 20, 7624 Pécs, Hungary<sup>3</sup> ELI-ALPS, ELI-Hu Nonprofit Ltd., Wolfgang Sandner u 3, 6728 Szeged, Hungary<sup>4</sup> MTA-PTE High-Field Terahertz Research Group, Ifjúság ú. 6, 7624 Pécs, Hungary

\* Correspondence: hebling@fizika.ttk.pte.hu

**Abstract:** We report a semiconductor contact grating terahertz source design based on a rectangular profile for phase-matched terahertz generation in the long infrared pump wavelength range. The calculations show that the best diffraction efficiency can be achieved by a filling factor significantly smaller than 50%. Furthermore, the possibility of diffraction efficiency enhancement was investigated by applying three different antireflective coating structures. Numerical simulations have indicated that at 2.06  $\mu\text{m}$  and 3.0  $\mu\text{m}$  pump wavelength, diffraction efficiencies greater than 91% and 89% can be achieved by adding an appropriate antireflective coating to the GaP and GaAs contact grating structure, respectively. In addition, numerical simulations were performed to investigate the influence of wall angles on diffraction efficiency. The results reveal that the wall angle does not significantly affect the diffraction efficiency: while keeping the wall angle deviation from the vertical below 25 degrees, the efficiency drop remains below 5% for otherwise optimal grating parameters.

**Keywords:** contact grating; diffraction efficiency; antireflective coating; gallium phosphide; gallium arsenide; terahertz pulses



**Citation:** Tibai, Z.; Mbithi, N.M.; Almási, G.; Fülöp, J.A.; Hebling, J. Design of Semiconductor Contact Grating Terahertz Source with Enhanced Diffraction Efficiency. *Crystals* **2022**, *12*, 1173. <https://doi.org/10.3390/cryst12081173>

Academic Editor: Arcady Zhukov

Received: 22 July 2022

Accepted: 17 August 2022

Published: 21 August 2022

**Publisher's Note:** MDPI stays neutral with regard to jurisdictional claims in published maps and institutional affiliations.



**Copyright:** © 2022 by the authors. Licensee MDPI, Basel, Switzerland. This article is an open access article distributed under the terms and conditions of the Creative Commons Attribution (CC BY) license (<https://creativecommons.org/licenses/by/4.0/>).

## 1. Introduction

High-energy terahertz pulses with a frequency range of 0.1–10 THz have wide applications in various research fields such as spectroscopy, sensing biological components, medical imaging, and material science [1–5]. Optical rectification occurs in nonlinear crystals such as lithium niobate (LN), semiconductors, and organic crystals, which are possible high-energy THz sources. Moreover, an effective optical rectification technique needs (as in every nonlinear optical frequency conversion process) phase matching or velocity matching. In the case of organic crystals and at the beginning of semiconductors, velocity matching was achieved by choosing an appropriate pump wavelength [6–8]. The tilting-pulse-front-pumping (TPFP) technique was proposed as a general method to achieve velocity matching in optical rectification in the THz range below the phonon–polariton frequency and demonstrated for GaP and LN [9].

TPFP was very effective in LN, resulting in single-cycle THz pulses with  $\mu\text{J}$  level energy [10]. Since THz pulses with this energy are suitable as the pump in THz pump–probe measurements, TPFP pumped LN THz sources have become very popular. Recently, the generation of terahertz pulses with as high as 1.4 mJ energy was demonstrated by this method [11]. However, in the conventional TPFP LN THz source, a prism-shaped LN crystal has to be used, limiting the beam quality of the generated THz radiation [12]. Therefore, the so-called contact grating (CG) setup was proposed to solve the problem in 2008 [13]. The first LN CG THz pulse source was designed in detail [14,15] and demonstrated [16]. However, because of technical reasons relating to the requirement of a large pulse front tilt in the case of the LN THz source, the achieved THz generation efficiency was an order of magnitude smaller than in the case of the conventional TPFP LN source.

It was recognized early that the efficiency of semiconductor THz sources could be increased by using long-wavelength pumping to eliminate low-order multiphoton absorption, which creates free carriers, causing THz absorption [17–20]. Detailed ZnTe semiconductor CG THz source design for long-wavelength pumping has been reported for rectangular and sinusoidal grating profiles [21,22]. Recently, such a source was produced successfully using a combination of electron lithography and reactive ion etching [23]. Good-quality CG with a close to rectangular profile (vertical walls), as large as 0.3% conversion efficiency, scalability of the THz energy, and perfect focusability of the THz beam was demonstrated. However, the small bubbles inside the ZnTe mean serious technical difficulties during the lithography process. GaP as an alternative for long-wavelength pumped CG semiconductor THz sources has been considered [24]. Recently, a broadband high-sensitivity time-resolved THz system consisting of a 1.03  $\mu\text{m}$  pumped GaP CG source and a GaP CG detector was reported [25]. The technical details of the GaP CG production are described in Ref. [26]. According to our recent investigations, GaP pumped at 2.06  $\mu\text{m}$  and GaAs pumped at 3.0  $\mu\text{m}$  are promising, highly efficient THz sources [27].

In this article, we use numerical simulations to design optimal CG GaP and GaAs THz sources pumped at 2.06  $\mu\text{m}$  and 3.0  $\mu\text{m}$ , respectively. At these wavelengths, five-photon and four-photon absorption are the lowest-order multiphoton absorption processes in GaP and GaAs, respectively. Furthermore, we investigate three methods for increasing the expected diffraction efficiency of the useful  $\pm 1$  diffraction orders from 60–70% to more than 88–90%.

## 2. Grating Design

Figure 1a illustrates the scheme of the contact grating with the laser pump beam incident normally to the grating surface. In the design, the pulse-front tilt angle  $\gamma$  was calculated from the velocity matching equation given by

$$\cos(\gamma) = \frac{n_g}{n_{THz}} \quad (1)$$

where  $n_g$  is the group index at the pump wavelength, and  $n_{THz}$  is the THz index [9]. The grating profile parameters were set according to the basic grating equation [21], which at normal incidence reduces to

$$n_p \sin(\beta_m) = \pm m \lambda_p / d \quad (2)$$

where  $d$  is the grating period,  $n_p$  is the refractive index of GaP or GaAs at the  $\lambda_p$  pump wavelength,  $\beta_m$  is the diffraction angle and  $m$  is the diffraction order. During the design, pump wavelengths of 2.06  $\mu\text{m}$  and 3.0  $\mu\text{m}$  were considered for GaP and GaAs, respectively. At 2.06  $\mu\text{m}$  pump wavelength, the indices of GaP were  $n_p(\lambda_p) = 3.036$  and  $n_g(\lambda_p) = 3.086$ , calculated from an equation obtained from Ref. [28], and the THz index  $n_{THz}(\lambda_{THz}) = 3.36$  was calculated (3 THz frequency was supposed) from an equation obtained from Ref. [29]. At 3.0  $\mu\text{m}$  pump wavelength, the indices of GaAs were  $n_p(\lambda_p) = 3.335$  and  $n_g(\lambda_p) = 3.383$ , calculated from an equation obtained from Ref. [30], and the THz index  $n_{THz}(\lambda_{THz}) = 3.65$  was calculated (3 THz frequency was supposed) from an equation obtained from Ref. [31]. The grating period  $d$  was chosen so that the  $\beta_1$  diffraction angle for the  $\pm 1$ st order would be equal to the  $\gamma$  angle needed for velocity matching according to Equation (1). Both for GaP and GaAs, there are  $\pm 2$ nd orders beside the  $\pm 1$ st and 0th orders. However, we considered only the sum of the  $\pm 1$ st diffraction orders as the diffraction efficiency since only those diffracted beams fulfilled the velocity matching condition, thus yielding THz generation. We investigated the effect of the possible distortion of the rectangular grating profile into a trapezoidal one as a result of imperfect manufacturing.

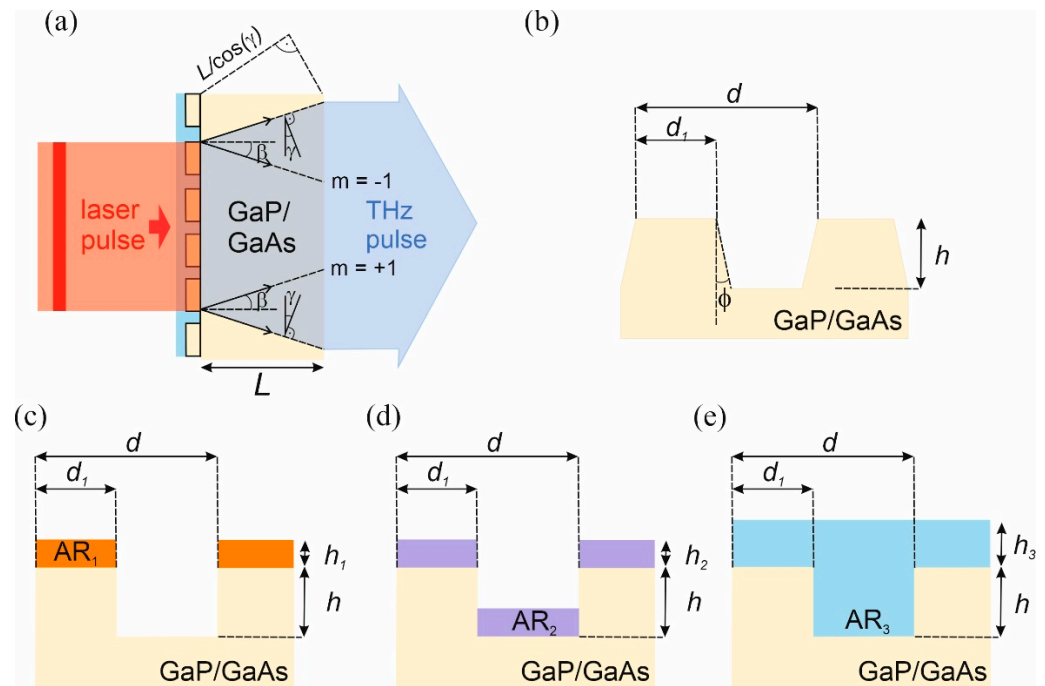


**Figure 1.** (a) Scheme of contact grating THz source. (b) Cross-section of a distorted grating profile indicating the  $\phi$ -wall angle. (c–e) Rectangular profiles with antireflective (AR) coatings of  $n_{AR_1} = n_{SiO_2}$ ,  $n_{AR_2} = \sqrt{n_{GaP/GaAs}}$ , and a Norland optical adhesive 170 (NOA), respectively.  $d$ —grating period,  $d_1$ —ridge width,  $h$ —groove depth,  $h_1$ — $AR_1$  thickness,  $h_2$ — $AR_2$  thickness,  $h_3$ — $AR_3$  thickness,  $n_{GaP/GaAs}$ —refractive index of GaP/GaAs, and  $L$ —crystal length.

To find methods to minimize Fresnel losses on the CG surface and to enhance the diffraction efficiency, the effect of three different types of “antireflection coating” (ARC) (see Figure 1c–e) were numerically investigated. The first one (see Figure 1c) can be achieved by just using appropriate  $SiO_2$  coating thickness in the first step and finishing the processes after the 7th step in the 8-step fabrication process based on contact photolithography illustrated in Figure 1 of Ref. [26]. The usual evaporation technique can create the second type of ARC (Figure 1d), while the third one (Figure 1e) occurs by overfilling the grooves with NOA and, after UV curing the NOA, polishing it to the needed  $h_3$  thickness. For the case of the first type of ARC (Figure 1c),  $SiO_2$  was supposed to be the ARC material ( $AR_1$ ). For the second and third types of ARC (Figure 1d,e), materials with a refractive index equal to the square root of the refractive index of the CG (GaP or GaAs) and NOA, respectively, were supposed to be the ARC materials. For starting, the antireflective coatings’ layer thicknesses  $h_1$ ,  $h_2$ , and  $h_3$  were supposed to be

$$h_1 = h_2 = h_3 = \frac{\lambda_p}{4n} \quad (3)$$

where  $n$  is the refractive index of the antireflective coating material. However, the thicknesses were scanned around these starting values.

### 3. Results

The diffraction efficiency for any given wavelength and polarization depends on the grating profile, the ridge width ( $d_1 = f \times d$ , where  $f$  is the filling factor), and groove depth  $h$  [32]. The  $d$  grating period was chosen so that the velocity matching condition (Equation (1)) would be fulfilled for both GaP and GaAs at the supposed 2.06  $\mu\text{m}$  and 3.0  $\mu\text{m}$  pump wavelength, respectively, and 3 THz generating frequency:  $d_{GaP} = 1.7 \mu\text{m}$ ,  $d_{GaAs} = 2.4 \mu\text{m}$ ; the corresponding pulse front tilt  $\gamma$  angles and diffraction  $\beta$  angles are:  $\gamma = \beta = 23.46^\circ$  for GaP and  $\gamma = \beta = 22.03^\circ$  for GaAs. Running the  $h$  and  $f$  parameters

on a broad range, numerical simulations of the efficiencies of all possible transmitted and reflected diffraction orders were performed on gratings with and without layers of antireflective coating in the transverse electric field (TE) polarization state (the electric field is parallel with the grooves). The choice of TE polarization over transverse magnetic field (TM) polarization is due to the fact that in TE, the effective nonlinear coefficient is about 30% larger; hence, 60% higher THz generation efficiency is predicted [33]. The numerical simulations were carried out using COMSOL Multiphysics software, and were based on the finite element methods' numerical solutions of partial differential equations [34]. The simulations were conducted to determine the set of parameters that yield maximum efficiency in the  $\pm 1$  diffraction order to provide a guideline for the fabrication.

### 3.1. Effect of Wall Angle on Diffraction Efficiency

Numerical simulations were carried out to investigate the influence of wall angle  $\phi$  (see Figure 1b) on the diffraction efficiency in the trapezoidal profiles. The highest diffraction efficiencies were determined by optimizing the groove depth  $h$  and filling factor  $f$  for each  $\phi$  wall angle. Figure 2a shows a contour plot of calculated diffraction efficiencies for GaP as a function of  $f$  and  $h$  at 3 THz phase-matching frequency, at a wall angle  $\phi = 0^\circ$  and at a pump wavelength of  $2.06 \mu\text{m}$ . A maximum diffraction efficiency of 74% was realized with a corresponding optimum groove depth and filling factor of  $h \approx 0.45 \mu\text{m}$  and  $f \approx 42.5\%$ , respectively. Considering the wall angle dependence, it can be observed in Figure 2b that at higher filling factors (greater than 27%), the diffraction efficiency decreases monotonically from the perpendicular wall (wall angle of  $\phi = 0^\circ$ , perfect rectangular grating profile). However, the decrease in the efficiency with the wall angle is very modest; the decrease is less than 5%, even for  $\phi = 25^\circ$  wall angle. On the other hand, at low filling factors (less than 25%), the diffraction efficiency increases monotonically with the wall angle up to a maximum value close to 74% at  $\phi = 20^\circ$ , followed by a monotonical decrease with the wall angle. The manufacturing of CG with a higher filling factor is recommended.

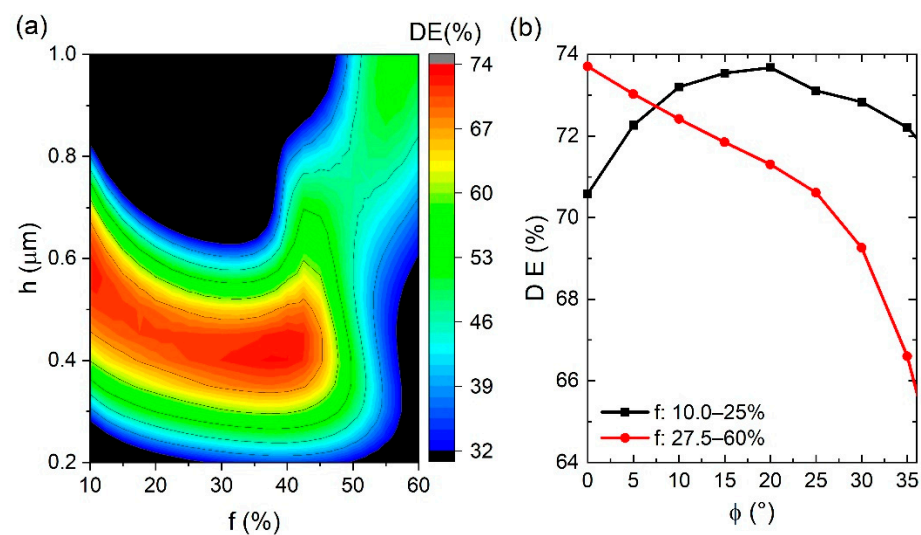


**Figure 2.** (a) Calculated GaP diffraction efficiency (DE) as a function of groove depth  $h$  and filling factor  $f$ , at perfect rectangular grating shape (wall angle,  $\phi = 0^\circ$ ) and (b) diffraction efficiency (DE) versus various wall angles  $\phi$ , at  $\lambda_p = 2.06 \mu\text{m}$ ,  $d = 1.7 \mu\text{m}$ , and 3 THz phase-matching frequency for TE polarization state.

### 3.2. Increasing Diffraction Efficiency by AR Coatings

The effect of adding an antireflective coating to the CG groove profiles on diffraction efficiency was investigated using numerical calculations for three cases. In the first case, we considered adding a layer of  $\text{SiO}_2$  on the ridges of the rectangular grating profile, as shown in Figure 1c. A diffraction efficiency close to 76% can be attained by adding  $\text{SiO}_2$  as an antireflective coating with the  $h_1 = 360 \text{ nm}$  coating thickness calculated from

Equation (3), using the refractive index value  $n_{\text{SiO}_2} = 1.437$ . The corresponding groove depth and filling factor were  $h \approx 0.40 \mu\text{m}$ , and  $f \approx 42.5\%$ , respectively, for a wavelength of  $2.06 \mu\text{m}$ . This is shown in Figure 3a by the contour plot of the calculated diffraction efficiencies for the GaP CG with a groove spacing,  $d = 1.7 \mu\text{m}$  as a function of filling factor  $f$ , and groove depth  $h$ , at a phase-matching frequency of 3 THz. To optimize the diffraction efficiency further, the antireflective coating layer thickness  $h_1$  was optimized numerically by varying coating thickness while keeping the optimum filling factor and groove depth fixed. Figure 3b shows a plot of diffraction efficiency versus the optimized antireflective coating thickness  $h_1$ . This optimization resulted in an additional 0.8% increase in the diffraction efficiency at  $h_1 = 280 \text{ nm}$ . We also performed numerical calculations using  $\text{Al}_2\text{O}_3$  as an antireflective coating. Since the index of refraction of  $\text{Al}_2\text{O}_3$  is very close to the square root of the refractive index of GaP, we expected a higher efficiency for this case. However, the diffraction efficiency obtained was only slightly higher (about 1%) than those obtained with  $\text{SiO}_2$ .

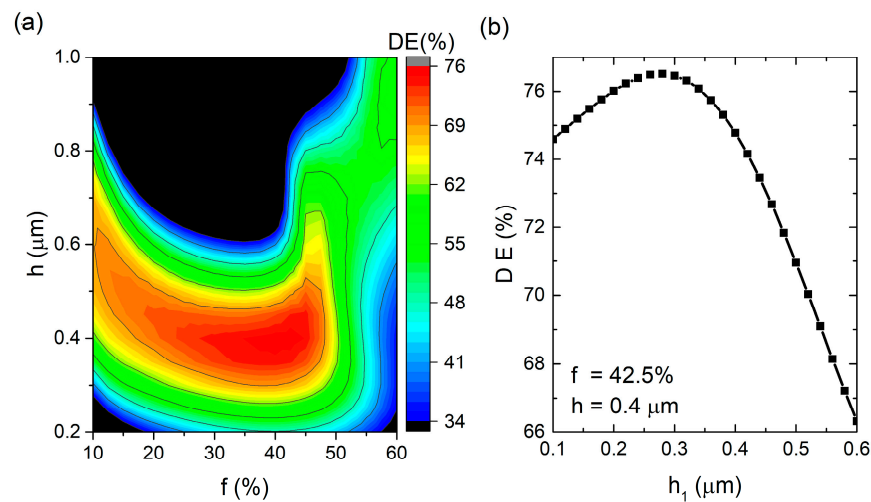


**Figure 3.** (a) Calculated GaP diffraction efficiency (DE) as a function of groove depth  $h$  and filling factor  $f$ , with  $h_1=360 \text{ nm}$  thick  $\text{SiO}_2$  ARC, and (b) diffraction efficiency (DE) versus  $\text{SiO}_2$ ARC thickness ( $h_1$ ), at  $\lambda_p = 2.06 \mu\text{m}$ ,  $d = 1.7 \mu\text{m}$ , and 3 THz phase-matching frequency.

In the second case, we considered adding an ARC layer having  $n_{\text{AR}_2} = \sqrt{n_{\text{GaP}}}$  on the rectangular grating profile, as shown in Figure 1d. Diffraction efficiencies close to 90% were attained, with corresponding groove depth and filling factor ranges of  $h \approx 0.47$  to  $0.51 \mu\text{m}$ , and  $f \approx 25$  to  $35\%$ , respectively, for a wavelength of  $2.06 \mu\text{m}$ , as illustrated in Figure 4a. The antireflective coating layer thickness  $h_2$  was optimized numerically by varying coating thickness while keeping the optimum filling factor and groove depth fixed. Figure 4b shows a plot of diffraction efficiency versus the ARC layer thickness  $h_2$ . The maximum diffraction efficiency of 90% was achieved with optimal filling factor,  $f = 30\%$ , and optimum groove depth,  $h = 0.49 \mu\text{m}$ . In this case, we found that  $h_2=320 \text{ nm}$  optimal AR thickness was almost equal with the  $300 \text{ nm}$  obtained from Equation (3).

In the third case, we considered adding a layer of NOA as an ARC on a rectangular grating profile, as shown in Figure 1e. Figure 5a shows a contour plot of the calculated diffraction efficiencies as a function of groove depth  $h$  and filling factor  $f$ . Diffraction efficiencies larger than 90% can be achieved over the optimal ranges of  $h \approx 0.70$  to  $0.80 \mu\text{m}$  and  $f \approx 27$  to  $37\%$ . The antireflective coating layer thickness  $h_3$  was optimized numerically by varying coating thickness while keeping the optimum filling factor and optimum groove depth fixed at  $f = 32.5\%$  and  $h = 0.75 \mu\text{m}$ , respectively, as illustrated in Figure 5b. This resulted in a maximum diffraction efficiency of as high as 92%, with  $f = 32.5\%$  and  $h = 0.75 \mu\text{m}$  as the optimal parameters.

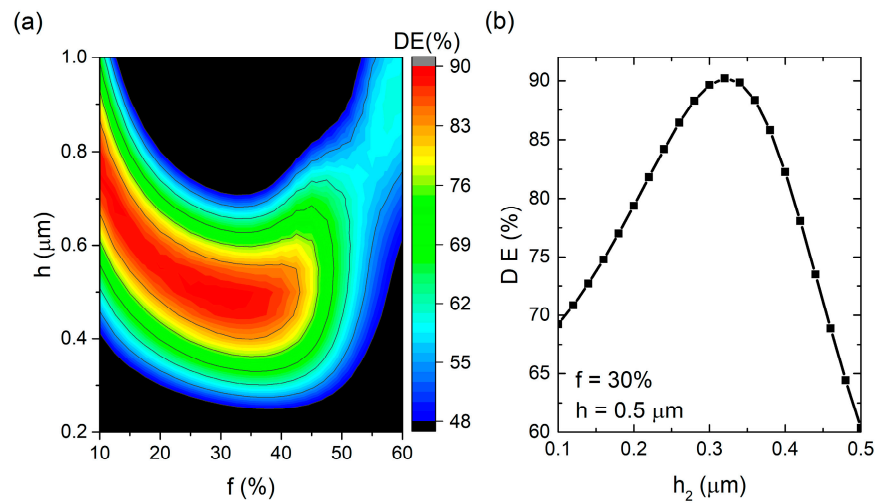


**Figure 4.** (a) Calculated GaP diffraction efficiency (DE) as a function of groove depth  $h$  and filling factor  $f$ , with  $h_2=300$  nm thick  $n_{AR_2} = \sqrt{n_{GaP}}$  ARC and (b) diffraction efficiency (DE) versus ARC thickness ( $h_2$ ), at  $\lambda_p = 2.06 \mu\text{m}$ ,  $d = 1.7 \mu\text{m}$ , and 3 THz phase-matching frequency.

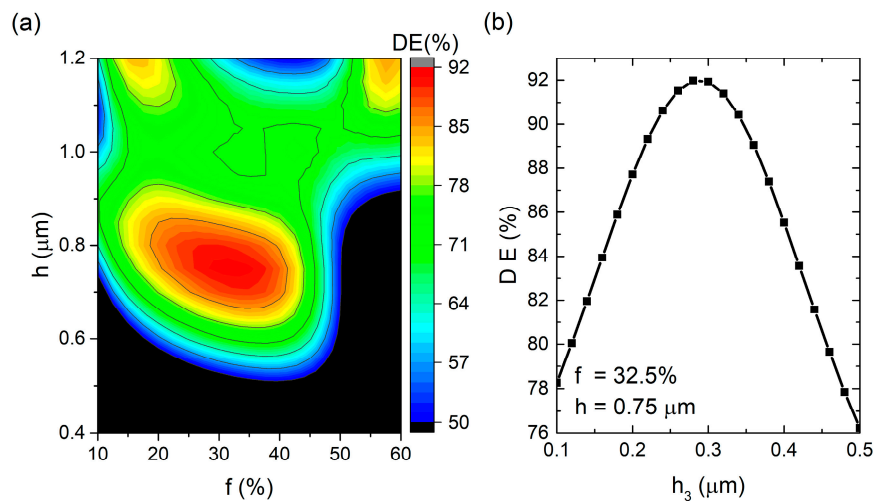


**Figure 5.** (a) Calculated GaP diffraction efficiency (DE) as a function of groove depth  $h$  and filling factor  $f$ , with  $h_3 = 315$  nm thick NOA ARC and (b) Diffraction efficiency versus NOA ARC thickness ( $h_3$ ), at  $\lambda_p = 2.06 \mu\text{m}$ ,  $d = 1.7 \mu\text{m}$ , and 3 THz phase-matching frequency.

Numerical calculations were performed to investigate the effect of adding an antireflective coating on the diffraction efficiencies of GaAs CG, too. Three cases similar to those performed on GaP were considered. The results indicate similar behavior as for GaP, but adding ARC resulted in a larger diffraction efficiency increase. This larger increase in GaAs is associated with a higher refractive index and a higher corresponding Fresnel loss in GaAs than GaP. For example, by adding a layer of  $n_{AR_2}$  antireflective coating to GaAs CG grating, the diffraction efficiency increased from 69% to 88%. This is a relative increase of 27%. Figure 6a,b display the plots of diffraction efficiency as a function of filling factor and groove depth without and with ARC with  $d = 2.4 \mu\text{m}$ , at a  $3.0 \mu\text{m}$  and 3 THz phase-matching frequency. The corresponding optimal parameters are as follows: without ARC,  $h \approx 0.54 \mu\text{m}$  and  $f \approx 39\%$ , while with ARC,  $h \approx 0.62 \mu\text{m}$  and  $f \approx 31\%$ , respectively. The effects of adding  $\text{SiO}_2$  and NOA antireflective coatings on the diffraction efficiency of GaAs CG are illustrated in Appendix A.

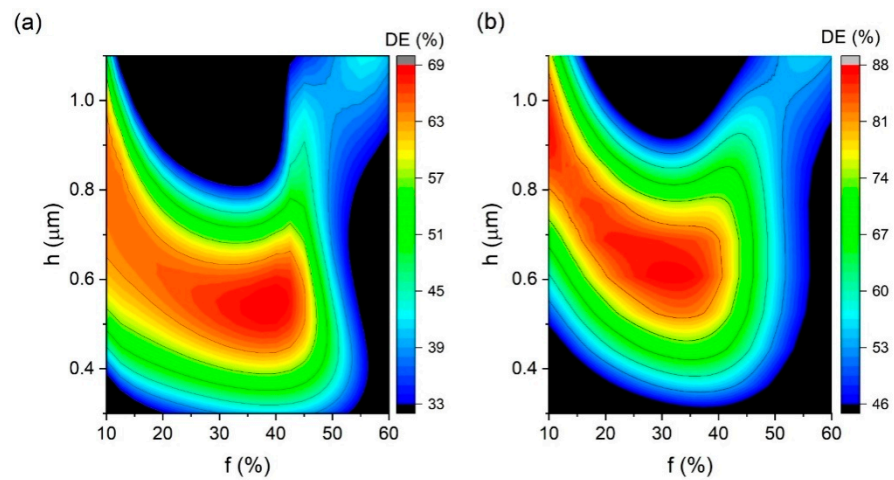


**Figure 6.** (a) Calculated GaAs diffraction efficiency (DE) as a function of groove depth  $h$  and filling factor  $f$  without ARC and (b) Calculated GaAs diffraction efficiency (DE) as a function of groove depth  $h$  and filling factor  $f$  with  $h_2 = 410$  nm thick  $n_{AR_2} = \sqrt{n_{GaAs}}$  ARC at  $\lambda_p = 3.0$   $\mu\text{m}$ ,  $d = 2.4$   $\mu\text{m}$ , and 3 THz phase-matching frequency.

#### 4. Discussion

The main results of our calculations are summarized in Table 1. In columns 1–7 are indicated: the material of the CG, the ARC type and material, the index of refraction of the ARC material, the filling factor, the depth of the grooves, the sum of the calculated diffraction efficiencies of the  $\pm 1$ st-order beams when the thickness of the ARC is chosen according to Equation (3), and the sum of the calculated diffraction efficiencies of the  $\pm 1$ st diffraction order beams when the thickness of the ARC is optimized for achieving the largest diffraction efficiency of the first-order beams.

**Table 1.** Summary of calculated diffraction efficiencies and their corresponding parameters.

Material	ARC	$n$	$f$ (%)	$h$ (nm)	DE(%)	Optimized DE(%)
GaP	—	—	42	430	74.2	—
	$AR_1(\text{SiO}_2)$	1.44	42.5	400	75.7 ( $h_1 = 360$ nm)	76.5 ( $h_1 = 280$ nm)
	$AR_1(\text{Al}_2\text{O}_3)$	1.73	37.5	350	77.0 ( $h_1 = 350$ nm)	77.4 ( $h_1 = 260$ nm)
	$AR_2(n_{AR_2} = \sqrt{n_{GaP}})$	1.74	30	490	89.8 ( $h_2 = 300$ nm)	90.2 ( $h_2 = 320$ nm)
	$AR_3(\text{NOA})$	1.64	32.5	750	91.6 ( $h_3 = 315$ nm)	91.9 ( $h_3 = 300$ nm)
GaAs	—	—	39	540	69.0	—
	$AR_1(\text{SiO}_2)$	1.42	37.5	500	72.2 ( $h_1 = 530$ nm)	72.5 ( $h_1 = 460$ nm)
	$AR_2(n_{AR_2} = \sqrt{n_{GaAs}})$	1.83	31	620	88.0 ( $h_2 = 410$ nm)	88.6 ( $h_2 = 440$ nm)
	$AR_3(\text{NOA})$	1.62	27.5	1000	89.6 ( $h_3 = 460$ nm)	89.8 ( $h_3 = 460$ nm)

GaP parameters are calculated at 2.06  $\mu\text{m}$ , and GaAs parameters are calculated at 3.0  $\mu\text{m}$ .

Before discussing the effects of the ARCs, it is important to notice that both in the case of bare CG and in the case of CG with any type of ARC, the highest diffraction efficiency of the first-order beams is achieved at a filling factor of less than 50%. Although the simple linear system formulation of nonparaxial scalar diffraction theory of rectangular phase gratings predicts maximum diffraction efficiency of the first order for a 50% filling factor [35], it is well known that the transmission gratings used in the Littrow arrangement have a maximum diffraction efficiency at a filling factor of less than 50% [36]. Furthermore, in the case of non-normal incidence, numerical simulations of LN and ZnTe rectangular CGs also predict a maximum diffraction efficiency for a filling factor of less than 50% [15,21]. However, this was not mentioned for normal incidence in the simulation work [21], and in all realizations of semiconductor CG contact gratings, a 50% filling factor was applied [23,25,26]. Therefore, we find it important to emphasize that a filling factor

of less than 50% resulted in the highest diffraction efficiency for normal incidence, too, as Figure 2a demonstrates.

In Ref. [37], the authors explained the working of rectangular phase transmission gratings by considering the two propagating modes inside the grating structure and taking into account their relative accumulated phase difference inside the grating and their overlap integral with the pumping. Although a quantitative explanation of the results based on a theory is beyond the scope of this paper, we note that an explanation should be possible in our case, too. Furthermore, evidence for the importance of the effect of the phase difference of the two modes (in the first, the “semiconductor mode” propagates predominantly inside the semiconductor, and in the second, the “air mode” propagates predominantly inside the air) is demonstrated in Figures 2a–4a and 6a, and in a less pronounced way in Figure 5a, too. The optimum groove depth increases with a decreasing filling factor in all these figures. This method can keep the phase difference between the two modes about fixed. With a smaller filling factor, a larger part of the electric field belonging to the “semiconductor mode” propagates inside air, and because of this, propagates faster. Thus, a longer path is needed to accumulate the same phase difference.

Considering the three investigated methods to increase the diffraction efficiency by decreasing the reflection loss, according to Table 1, the first method results in only about a 3% relative increase. This very modest improvement is reasonable since, in this case, ARC is present only on top of the narrow grooves. Yet, it is worth considering the application of this method since (as was mentioned above) it means not more but fewer process steps during the preparation of the CG.

The second (classical) ARC method results in much higher relative increases of 22% and 28% in the first-order diffraction efficiency for GaP and GaAs CG, respectively. Thus, we strongly suggest applying this method. Moreover, contrary to the first method, the optimized ARC thickness, in this case, is equal to the value predicted by Equation (3).

The application of the third ARC method results in even higher relative increases of 24% and 30% in the first-order diffraction efficiency for GaP and GaAs CG, respectively. These values are close to the 35% and 41% Fresnel losses of bare GaP and GaAs surfaces, respectively. Consequently, if technically possible, the adaptation of this method is very much recommended. A further advantage is that such a CG would also be more durable because of its flat surface.

The diffraction efficiency calculations were performed for monochromatic radiation; however, the CG THz sources were pumped with laser pulses having sub-hundred—few hundred fs duration and correspondingly large spectral bandwidth. In order to see the possible negative effect of the large bandwidth, for GaP CG optimized for 2.06  $\mu\text{m}$ , diffraction efficiency calculations were performed at 2.01 and 2.11  $\mu\text{m}$  as well. We obtained less than a 1% drop for these wavelengths compared to the 2.06  $\mu\text{m}$  case. Since the investigated 0.1  $\mu\text{m}$  spectral width can support 55 fs long pulses, we can conclude that our diffraction efficiency results are applicable for longer than 50 fs pump pulses.

Finally, we note that the application of any investigated ARC method needs a redesign of the (basic) CG structure (see Table 1). However, the parameters of the CG (groove depth and ridge width) with ARC do not differ drastically from the CG without ARC. The 85% increase in groove depth in the GaAs CG with the NOA ARC case is probably the most significant technical challenge. However, considering the 2.4 times larger grating period than the groove depth, the preparation of the CG with NOA also seems feasible.

## 5. Conclusions

We investigated, via numerical calculations, ways of increasing diffraction efficiency in semiconductor CG THz sources for the further upscaling of THz pulse energy and field strength in the long infrared pump wavelength range. Three different types of ARC structures were considered for decreasing the pump’s Fresnel reflection and increasing the diffraction efficiency of the  $\pm 1$ st-order beams, which are responsible for THz pulse generation. The parameters of the CG belonging to the highest diffraction efficiency differ



in the cases of having and not having ARC. Based on rectangular CG profiles, diffraction efficiencies greater than 91% and 89% can be realized in gallium phosphide and gallium arsenide, respectively, by adding an appropriate ARC on the gratings. The investigated methods can also be applied to other semiconductor contact gratings such as ZnSe and CdTe. The numerical calculations have also revealed that if the CG manufacturing results in a trapezoidal profile with less than a  $25^\circ$  wall angle, the diffraction efficiency drop remains below 5% for reoptimized grating parameters.

**Author Contributions:** Conceptualization, J.H. and J.A.F.; methodology, Z.T. and G.A.; validation, Z.T., J.H. and J.A.F.; investigation, Z.T. and N.M.M.; writing—original draft preparation, N.M.M. and J.H.; writing—review and editing, N.M.M., Z.T., G.A. and J.H.; visualization, N.M.M. and Z.T.; supervision, J.H.; funding acquisition, G.A., Z.T. and J.H. All authors have read and agreed to the published version of the manuscript.

**Funding:** National Research, Development, and Innovation Office (2018-1.2.1-NKP-2018-00010, TKP2021-EGA-17), and the Hungarian Scientific Research Fund (OTKA) (129134).

**Institutional Review Board Statement:** Not applicable.

**Informed Consent Statement:** Not applicable.

**Data Availability Statement:** The data supporting the findings of this study are available within this article.

**Acknowledgments:** Zoltán Tibai would like to thank the support of the János Bolyai Research Scholarship of the Hungarian Academy of Science.

**Conflicts of Interest:** The authors declare no conflict of interest.

## Appendix A

Figure A1a shows a plot of the calculated diffraction efficiencies as a function of groove depth  $h$  and filling factor  $f$  that result from adding a layer of  $\text{SiO}_2$  ARC on a GaAs CG for  $3.0\ \mu\text{m}$  pump wavelength and  $d = 2.4\ \mu\text{m}$  grating period at 3 THz phase-matching frequency. The maximum diffraction efficiency of 72.5% was achieved with optimal filling factor  $f = 37.5\%$  and optimum groove depth  $h = 0.5\ \mu\text{m}$ . Comparing Figure 6a (without ARC) with Figure A1a, a 5% relative increase in diffraction efficiency can be achieved.

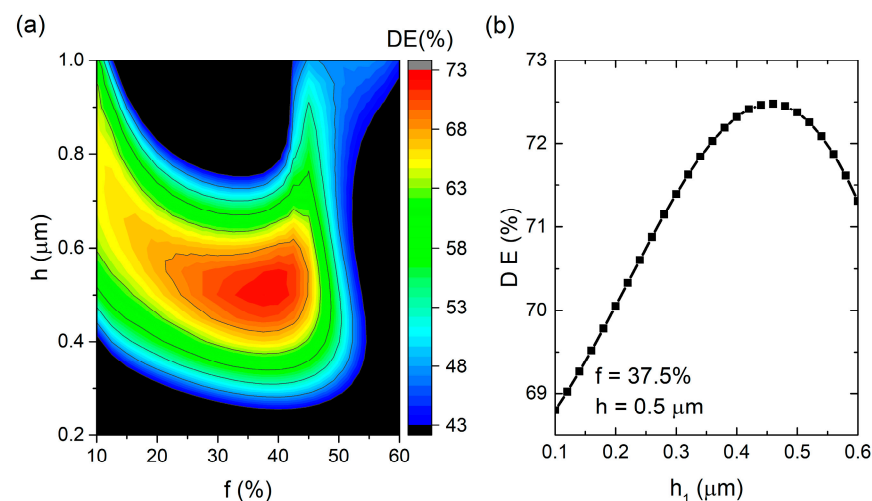


**Figure A1.** (a) Calculated GaAs diffraction efficiency (DE) as a function of groove depth  $h$  and filling factor  $f$ , with  $h_1 = 530\ \text{nm}$ -thick  $\text{SiO}_2$  ARC and (b) diffraction efficiency versus  $\text{SiO}_2$  ARC thickness ( $h_1$ ), at  $\lambda_p = 3.0\ \mu\text{m}$ ,  $d = 2.4\ \mu\text{m}$ , and 3 THz phase-matching frequency.

Figure A2a shows a plot of calculated diffraction efficiencies as a function of groove depth  $h$  and filling factor  $f$  that results from adding a layer of NOA as an ARC in GaAs

CG at 3.0  $\mu\text{m}$  pump wavelength,  $d = 2.4 \mu\text{m}$  grating period, and at 3 THz phase-matching frequency. The maximum diffraction efficiency of 89.6% was achieved with optimal filling factor  $f = 27.5\%$  and optimum groove depth  $h = 1 \mu\text{m}$ . Comparing Figure 6a (without ARC) with Figure A2a, a 30% relative increase in diffraction efficiency can be achieved.

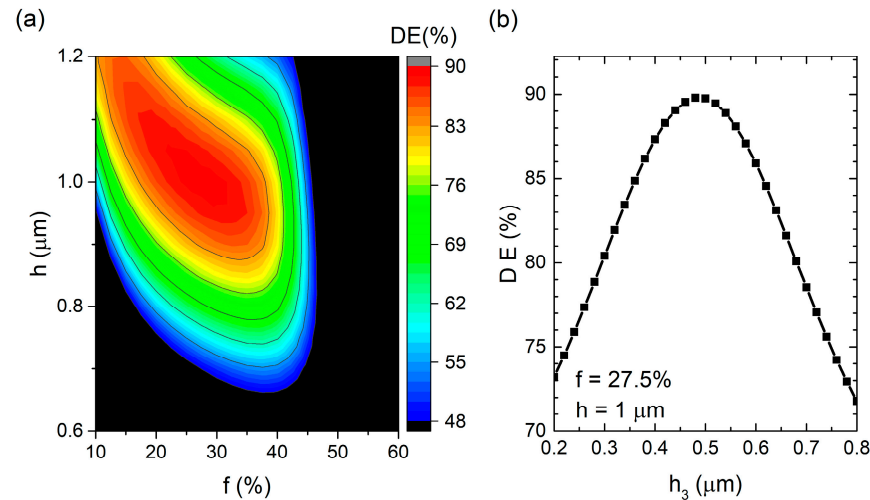


**Figure A2.** (a) Calculated GaAs diffraction efficiency (DE) as a function of groove depth  $h$  and filling factor  $f$ , with NOA ARC and (b) diffraction efficiency versus NOA ARC thickness  $h_3$ , at  $\lambda_p = 3.0 \mu\text{m}$ ,  $d = 2.4 \mu\text{m}$ , and 3 THz phase-matching frequency.

## References

1. Fischer, B.M.; Hoffmann, M.; Helm, H.; Wilk, R.; Rutz, F.; Kleine-Ostmann, T.; Koch, M.; Jepsen, P.U. Terahertz time-domain spectroscopy and imaging of artificial RNA. *Opt. Express* **2005**, *13*, 5205–5215. [[CrossRef](#)] [[PubMed](#)]
2. Jepsen, P.U.; Cooke, D.G.; Koch, M. Terahertz spectroscopy and Imaging-Modern techniques and applications. *Laser Photon. Rev.* **2011**, *5*, 124–166. [[CrossRef](#)]
3. Salén, P.; Basini, M.; Bonetti, S.; Hebling, J.; Krasilnikov, M.; Nikitin, A.Y.; Shamuilov, G.; Tibai, Z.; Zhaunerchyk, V.; Goryashko, V. Matter manipulation with extreme terahertz light: Progress in the enabling THz technology. *Phys. Rep.* **2019**, *836–837*, 1–74. [[CrossRef](#)]
4. Manikandan, E.; Princy, S.S.; Sreeja, B.S.; Radha, S. Structure Metallic Surface for Terahertz Plasmonics. *Plasmonics* **2019**, *14*, 1311–1319. [[CrossRef](#)]
5. Gupta, D.N. Optical Second-Harmonic Generation of Terahertz Field from n-type InSb Semiconductors. *Plasmonics* **2020**, *16*, 419–424. [[CrossRef](#)]
6. Vicario, C.; Jazbinsek, M.; Ovchinnikov, A.V.; Chefonov, O.V.; Ashitkov, S.I.; Agranat, M.B.; Hauri, C.P. High efficiency THz generation in DSTMS, DAST and OH1 pumped by Cr:forsterite laser. *Opt. Express* **2015**, *23*, 4573–4580. [[CrossRef](#)]
7. Vicario, C.; Monoszlai, B.; Hauri, C.P. GV/m Single-Cycle Terahertz Fields from a Laser-Driven Large-Size Partitioned Organic Crystal. *Phys. Rev. Lett.* **2014**, *112*, 213901. [[CrossRef](#)]
8. Nagai, M.; Tanaka, K.; Ohtake, H.; Bessho, T.; Sugiura, T.; Hirosumi, T.; Yoshida, M. Generation and detection of terahertz radiation by electro-optical process in GaAs using 1.56  $\mu\text{m}$  fiber laser pulses. *Appl. Phys. Lett.* **2004**, *85*, 3974–3976. [[CrossRef](#)]
9. Hebling, J.; Almási, G.; Kozma, I.Z.; Kuhl, J. Velocity matching by pulse front tilting for large area THz-pulse generation. *Opt. Express* **2002**, *10*, 1161–1166. [[CrossRef](#)]
10. Yeh, K.L.; Hoffmann, M.C.; Hebling, J.; Nelson, K.A. Generation of 10  $\mu\text{J}$  ultrashort terahertz pulses by optical rectification. *Appl. Phys. Lett.* **2007**, *90*, 171121. [[CrossRef](#)]
11. Zhang, B.; Ma, Z.; Ma, J.; Wu, X.; Ouyang, C.; Kong, D.; Hong, T.; Wang, X.; Yang, P.; Chen, L.; et al. 1.4-mJ High Energy Terahertz Radiation from Lithium Niobates. *Laser Photon. Rev.* **2021**, *15*, 2000295. [[CrossRef](#)]
12. Stepanov, A.G.; Hebling, J.; Kuhl, J. Efficient generation of subpicosecond terahertz radiation by phase-matched optical rectification using ultrashort laser pulses with tilted pulse fronts. *Appl. Phys. Lett.* **2003**, *83*, 3000–3002. [[CrossRef](#)]
13. Palfalvi, L.; Fülöp, J.A.; Almási, G.; Hebling, J. Novel setups for extremely high power single-cycle terahertz pulse generation by optical rectification. *Appl. Phys. Lett.* **2008**, *92*, 171107. [[CrossRef](#)]
14. Nagashima, K.; Kosuge, A. Design of Rectangular Transmission Gratings Fabricated in LiNbO<sub>3</sub> for High-Power Terahertz-Wave Generation. *Jpn. J. Appl. Phys.* **2010**, *49*, 122504. [[CrossRef](#)]
15. Ollmann, Z.; Hebling, J.; Almási, G. Design of a contact grating setup for mJ-energy THz pulse generation by optical rectification. *Appl. Phys. B-Lasers O* **2012**, *108*, 821–826. [[CrossRef](#)]

16. Tsubouchi, M.; Nagashima, K.; Yoshida, F.; Ochi, Y.; Maruyama, M. Contact grating device with Fabry–Perot resonator for effective terahertz light generation. *J. Opt. Lett.* **2014**, *39*, 5439–5442. [[CrossRef](#)] [[PubMed](#)]
17. Hoffmann, M.C.; Yeh, K.L.; Hebling, J.; Nelson, K.A. Efficient terahertz generation by optical rectification at 1035 nm. *Opt. Express* **2007**, *15*, 11706–11713. [[CrossRef](#)]
18. Hebling, J.; Yeh, K.L.; Hoffmann, M.C.; Bartal, B.; Nelson, K.A. Generation of high-power terahertz pulses by tilted-pulse-front excitation and their application possibilities. *J. Opt. Soc. Am. B* **2008**, *25*, B6–B19. [[CrossRef](#)]
19. Blanchard, F.; Schmidt, B.E.; Ropagnol, X.; Thiré, N.; Ozaki, T.; Morandotti, R.; Cooke, D.G.; Légaré, F. Terahertz pulse generation from bulk GaAs by a tilted-pulse-front excitation at 1.8  $\mu\text{m}$ . *Appl. Phys. Lett.* **2014**, *105*, 241106. [[CrossRef](#)]
20. Vodopyanov, K.L. Optical THz-wave generation with periodically-inverted GaAs. *Laser Photon. Rev.* **2008**, *2*, 11–25. [[CrossRef](#)]
21. Ollmann, Z.; Fülöp, J.A.; Hebling, J.; Almási, G. Design of a high-energy terahertz pulse source based on ZnTe contact grating. *Opt. Commun.* **2014**, *315*, 159–163. [[CrossRef](#)]
22. Bakunov, M.I.; Bodrov, S.B. Terahertz generation with tilted-front laser pulses in a contact-grating scheme. *J. Opt. Soc. Am. B Opt. Phys.* **2014**, *31*, 2549–2557. [[CrossRef](#)]
23. Fülöp, J.A.; Polónyi, G.; Monoszlai, B.; Andriukaitis, G.; Balciunas, T.; Pugzlys, A.; Arthur, G.; Baltuska, A.; Hebling, J. Highly efficient scalable monolithic semiconductor terahertz pulse source. *Optica* **2016**, *3*, 1075–1078. [[CrossRef](#)]
24. Polonyi, G.; Mechler, M.I.; Hebling, J.; Fulop, J.A. Prospects of Semiconductor Terahertz Pulse Sources. *IEEE J. Sel. Top. Quantum Electron.* **2017**, *23*, 25–29. [[CrossRef](#)]
25. Cui, W.; Awan, K.M.; Huber, R.; Dolgaleva, K.; Ménard, J.M. Broadband and High-Sensitivity Time-Resolved THz System Using Grating-Assisted Tilted-Pulse-Front Phase Matching. *Adv. Opt. Mater.* **2022**, *10*, 2101136. [[CrossRef](#)]
26. Bashirpour, M.; Cui, W.; Gamouras, A.; Ménard, J.M. Scalable Fabrication of Nanogratings on GaP for Efficient Diffraction of Near-Infrared Pulses and Enhanced Terahertz Generation by Optical Rectification. *Crystals* **2022**, *12*, 684. [[CrossRef](#)]
27. Mbithi, N.M.; Tóth, G.; Tibai, Z.; Benabdelghani, I.; Nasi, L.; Krizsán, G.; Hebling, J.; Polonyi, G. Investigation of terahertz pulse generation in semiconductors pumped at long infrared wavelengths. *J. Opt. Soc. Am. B* **2022**, Submitted.
28. Wei, J.; Murray, J.M.; Barnes, J.O.; Krein, D.M.; Schunemann, P.G.; Guha, S. Temperature dependent Sellmeier equation for the refractive index of GaP. *Opt. Mater. Express* **2018**, *8*, 485–490. [[CrossRef](#)]
29. Parsons, D.F.; Coleman, P.D. Far Infrared Optical Constants of Gallium Phosphide. *Appl. Opt.* **1971**, *10*, 1683\_1681–1685. [[CrossRef](#)]
30. Kachare, A.H.; Spitzer, W.G.; Fredrickson, J.E. Refractive index of ion-implanted GaAs. *J. Appl. Phys.* **1976**, *47*, 4209–4212. [[CrossRef](#)]
31. Palik, E.D. *Handbook of Optical Constants of Solids*; Academic Press: Cambridge, MA, USA, 1998; Volume 3.
32. Nguyen, H.T.; Shore, B.W.; Bryan, S.J.; Britten, J.A.; Boyd, R.D.; Perry, M.D. High-efficiency fused-silica transmission gratings. *Opt. Lett.* **1997**, *22*, 142–144. [[CrossRef](#)] [[PubMed](#)]
33. Krizsán, G.; Tibai, Z.; Almási, G.; Tóth, G.; Pálfalvi, L.; Hebling, J. New Generation Terahertz Pulse Sources Utilizing Volume Phase Holographic Gratings. In Proceedings of the High Intensity Lasers and High Field Phenomena, Budapest, Hungary, 21–25 March 2022; p. HF3B.6. [[CrossRef](#)]
34. Zimmerman, W.B. *Multiphysics Modeling with Finite Element Methods*; World Scientific Publishing Co. Pte. Ltd.: Singapore, 2006; Volume 18.
35. Harvey, J.E.; Pfisterer, R.N. Understanding diffraction grating behavior: Including conical diffraction and Rayleigh anomalies from transmission gratings. *Opt. Eng.* **2019**, *58*, 087105. [[CrossRef](#)]
36. Clausnitzer, T.; Limpert, J.; Zöllner, K.; Zellmer, H.; Fuchs, H.J.; Kley, E.B.; Tünnermann, A.; Jupé, M.; Ristau, D. Highly efficient transmission gratings in fused silica for chirped-pulse amplification systems. *Appl. Opt.* **2003**, *42*, 6934–6938. [[CrossRef](#)] [[PubMed](#)]
37. Clausnitzer, T.; Kämpfe, T.; Kley, E.B.; Tünnermann, A.; Peschel, U.; Tishchenko, A.V.; Parriaux, O. An intelligible explanation of highly-efficient diffraction in deep dielectric rectangular transmission gratings. *Opt. Express* **2005**, *13*, 10448–10456. [[CrossRef](#)] [[PubMed](#)]